Analysis of the preliminary campaign for the PETALE program

Axel Laureau, Adrien Gruel, Vincent Lamirand, Thomas Ligonnet, Alix Sardet, Andreas Pautz

EPJ Nuclear Sci. Technol. **9**, 25 (2023)

https://doi.org/10.1051/epjn/2023010

EPJ Nuclear Sciences & Technologies

Available online at:
https://www.epj-n.org

REGULAR ARTICLE

OPEN ACCESS

Analysis of the preliminary campaign for the PETALE program

Axel Laureau[1,2,3,*], Adrien Gruel[4], Vincent Lamirand[3,5], Thomas Ligonnet[3], Alix Sardet[4], and Andreas Pautz[3,5]

[1] Laboratory for Reactor Physics and Systems behaviour (LRS), Ecole Polytechnique Fédérale de Lausanne (EPFL), 1015 Lausanne, Switzerland
[2] Univ. Grenoble Alpes, CNRS, Grenoble INP, LPSC-IN2P3, 38000 Grenoble, France
[3] SUBATECH, CNRS/IN2P3, IMT-Atlantique, 44307 Nantes, France
[4] CEA, DES, IRESNE, DER, Cadarache, 13108 Saint-Paul-Lez-Durance, France
[5] Nuclear Energy and Safety Research Division (NES), Paul Scherrer Institut (PSI), 5232 Villigen, Switzerland

Received: 10 November 2022 / Received in final form: 28 February 2023 / Accepted: 24 April 2023

Abstract. The PETALE program aims to provide new experimental data to constrain the stainless steel nuclear data. In this frame, a preliminary measurement campaign has been performed to characterize the neutron flux in key positions of the CROCUS reactor and to develop analysis tools. During this preliminary campaign detailed in the present paper, an efficiency ratio technique has been developed and tested to speed up HPGe measurements by a factor of 30. A second objective of the campaign concerns the propagation of nuclear data uncertainty from the core neutron cross-sections to the reaction rates in the dosimeters. Uncertainties in the core cross sections, such as the uranium cross section, are nuisance parameters that add uncertainty to the dosimeter reaction rate calculation. This component must be fully characterized with covariances to constrain the metal reflector component for Bayesian assimilation. The experimental results are compared to the calculations with different nuclear databases for the nuclear data uncertainty propagation. A good agreement is obtained with the ENDF/B-VII.1 database and a systematic underestimation of around 5–10% in the fast range is observed with the ENDF/B-VIII.0 and JEFF-3.3 databases.

1 Introduction

The objective of the PETALE program [1,2] is to provide new experimental data to constrain the stainless steel nuclear data. It consists of dosimeter activations and reactivity measurements using iron, nickel, and chromium metal reflector separately in the CROCUS reactor as presented in Figure 1. The measurement of reaction rates in a transmission experiment reduces the experimental uncertainties thanks to a strong correlation in-between the dosimeter's positions and types.

The preliminary campaign presented in this paper is collaborative work between EPFL and CEA to prepare the PETALE campaign. The first objective is to test the experimental procedure and the analysis process up to the calculation-experiment comparison, including covariances in-between the dosimeters in the uncertainty propagation. The second objective is to characterize the neutron flux in different positions of the CROCUS reactor. The campaign detailed here includes measurements in the reflector area with water replacing the PETALE device in the reflector. The measurements with the PETALE experiment are the object of the following campaign.

The present preliminary campaign has been performed during the fall of 2019. The experimental setup is presented in Section 2. Specific developments have been performed to optimize the High Purity Germanium (HPGe) measurements and to propagate the nuclear data uncertainty (Sect. 3). Finally, the experimental and calculation results are compared in Section 4 for different nuclear databases.

2 Experimental campaign presentation

A typical experimental setup in the CROCUS reactor is visible in Figure 2 for the axial nickel dosimeter measurement. Different irradiations have been performed with different powers and irradiation times, depending on the expected reaction rate, the decay constant, and the cooling time. The dosimeters are installed in three different positions:

– Core center: large plastic rod with a central region containing the dosimeters along the axial direction.

* e-mail: laureau.axel@gmail.com

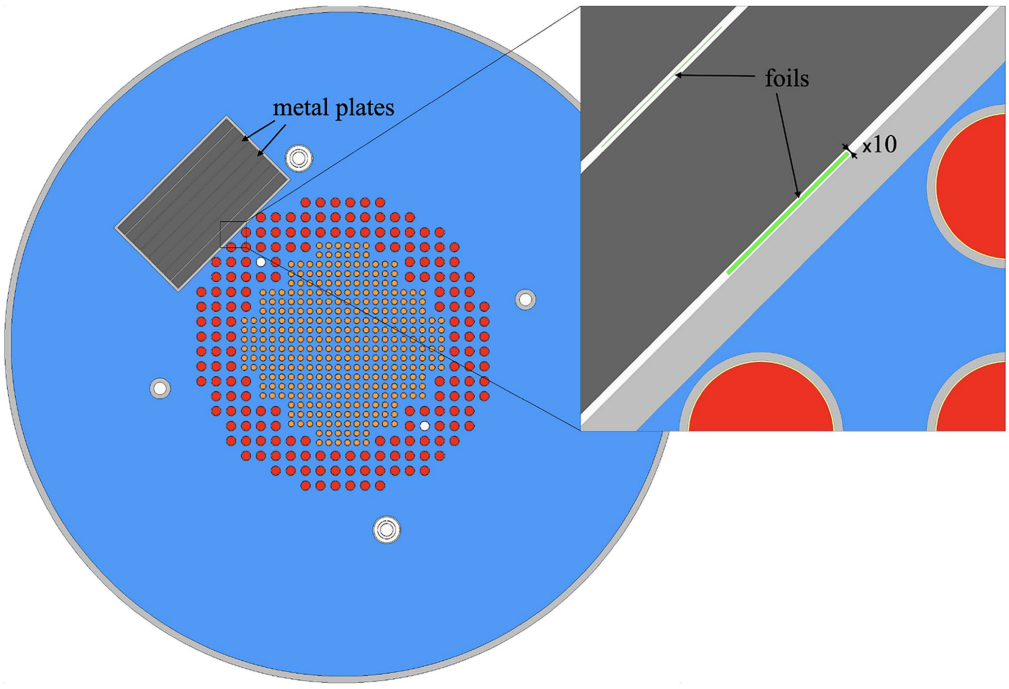

Fig. 1. CROCUS reactor with the PETALE experimental setup (top left) consisting of successive metal plates interspaced with dosimeter foils. The first foil thickness is multiplied by ten on the figure in order to be visible.

– Control rod: in the metallic fuel region (in red) and replacing a CROCUS control rod, a plastic rod with a cuboid shape holds dosimeters in the middle of the axial position.
– Reflector: a guide tube has been added for the measurements in the reflector close to the metallic fuel region, containing a plastic rod with dosimeters along the axial direction.

Note that the reflector position corresponds to the neutron arriving in the forefront position of the PETALE setup. This allows characterizing the neutron flux at this position, even if PETALE is a transmission experiment and thus not very sensitive to the local flux knowledge. A bad estimation of the local flux will be a first order nuisance parameter on absolute reaction rates, but a second order one on reaction rate comparisons (or ratios).

Different dosimeter types and positions have been measured. All the types are summarized in Table 1. For each type of dosimeter, a minimum of three measurements has been performed at mid-height (around 50 cm) for all the positions. For the gold and nickel dosimeters, respectively sensitive to thermal and fast neutrons, an axial flux measurement is performed as visible on the right of Figure 2 with a regular spacing in order to check the axial reconstruction.

Due to the different dosimeter cross sections, decay time, and HPGe management, the measurements correspond to four distinct irradiations from 1 hour up to 4 hours with a reactor power close to 30 W. The exact power and irradiation profile are monitored using fission chambers [3].

3 Analysis

The experimental analysis consists to link the experimental observable, here a number of counts in a High Purity Germanium (HPGe), to a reaction rate estimated with a neutron transport code. An important element is the estimation and propagation of all the uncertainties along the analysis. In previous studies, the algorithm and the software have been settled for the following steps:

– γ self–absorption in the dosimeters [3].
– HPGe efficiency calibration takes into account the input/output covariances with multiple calibration sources [3].
– Reconstruction of the irradiation and decay profile based on the reactor monitors (fission chambers) [3].
– Monte Carlo Serpent2 [4] (modified) calculation with variance reduction to estimate the reaction rates in the dosimeters [5].
– Propagation of the dosimetry nuclear data uncertainties from IRDFF-1.05 [3,6].
– Nuclear data Bayesian assimilation technique [7].

In order to complete the "Calculation/Experiment" (C/E) comparison, two elements have been added to the analysis process: the propagation of nuclear data uncertainties of the core modeling (*i.e.* uranium, moderator, influence of the structures) and the efficiency ratio for faster HPGe measurements. Both new elements are detailed below.

3.1 Uncertainty propagation of core cross-sections

Considering the neutron flux in the three different positions (axially integrated here), the spectrum calculated

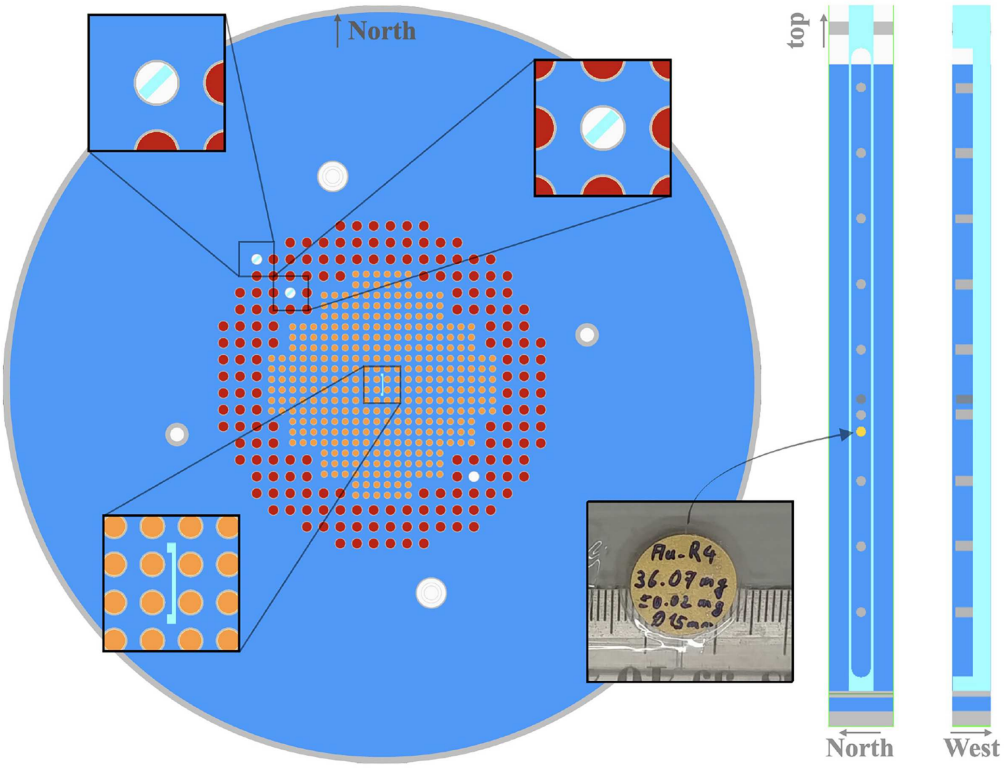

Fig. 2. Experimental setup in the CROCUS reactor (left) and axial visualization of the central plastic rod (right).

Table 1. Dosimeter description, classified according to the averaged lethargy of the neutron that interacts with the dosimeter at the core center position (column on the right).

Material	Reaction	Decay	Neutron energy
Iron	^{58}Fe (n,γ)	44.494 d	0.08 eV
Indium	^{115}In (n,γ)	54.29 m	0.15 eV
Gold	^{197}Au (n,γ)	2.69 d	0.4 eV
Indium	^{115}In (n,n$'$)	4.486 h	2.5 MeV
Nickel	^{58}Ni (n,p)	70.9 d	4.0 MeV
Iron	^{54}Fe (n,p)	312.20 d	4.3 MeV
Iron	^{56}Fe (n,p)	2.58 h	7.5 MeV
Aluminium	^{27}Al (n,α)	15.0 h	8.5 MeV

with the ENDF/B-VII.1 database is given in Figure 3. We can see that, as expected, the neutron flux is larger at the center position (blue curve) and lower in the reflector (red curve).

3.1.1 Cross-section sampling

In order to estimate the uncertainty of these spectra, we use the in-house Coconust code under development at CNRS to generate random samples of the ACE files. This sampling is based on the cross-section covariance matrices generated with NJOY [8] as presented in Figure 4 for ^{238}U.

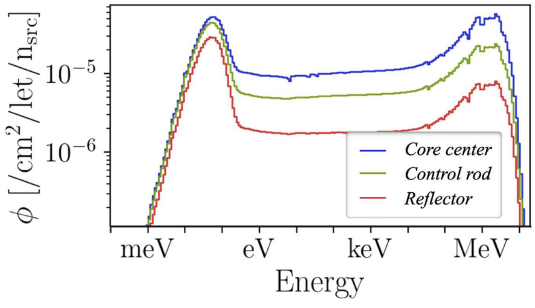

Fig. 3. Neutron spectrum in the different experimental positions.

Then random ACE files are generated according to these covariance matrices as illustrated in Figure 5.

3.1.2 Uncertainty propagation on the neutron spectrum

Finally these random ACE files are individually used in neutron transport calculation in order to obtain a variation on the different variables of interest (multiplication factor, flux, spectrum...). For this study, the procedure is performed 32 times, perturbing ^{235}U and ^{238}U (elastic, total inelastic, fission, capture, delayed, and prompt multiplicities), ^{27}Al (elastic, total inelastic, capture), ^{16}O and ^{1}H (elastic, capture). This list comes from the main components of the materials in the core during the first

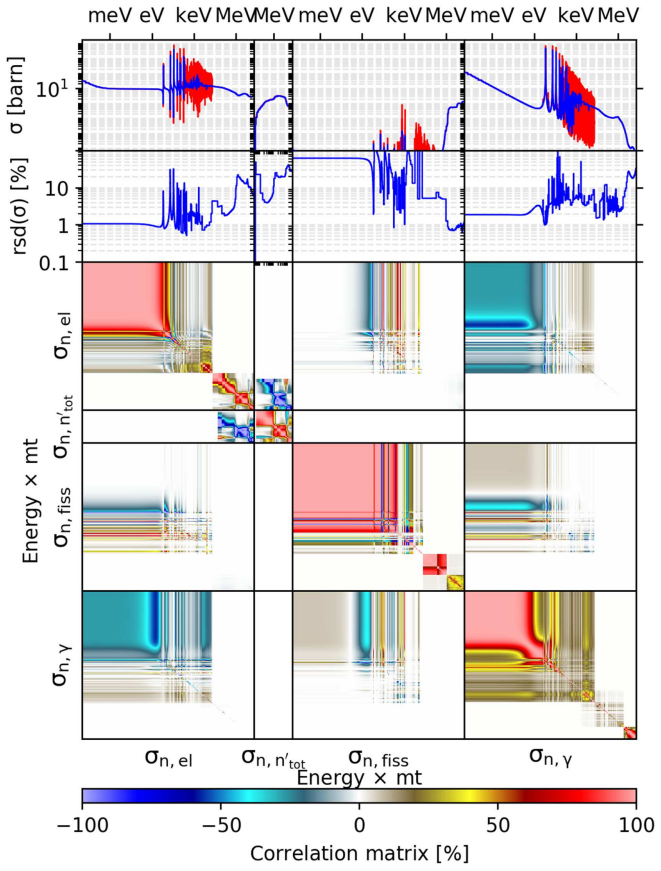

Fig. 4. Cross-section covariance matrix of ^{238}U (ENDF/B-VII.1).

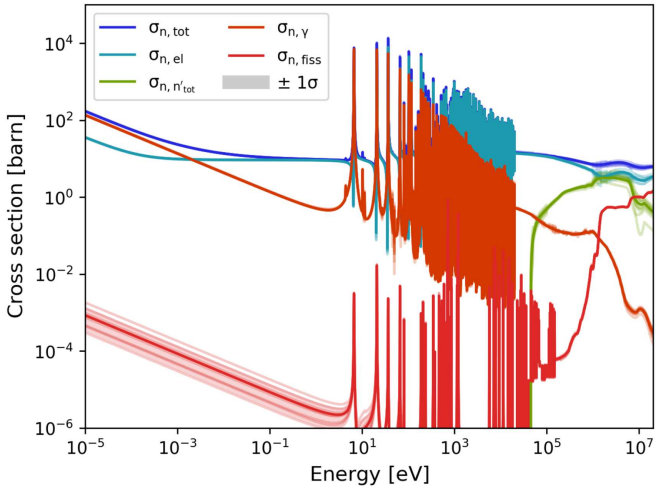

Fig. 5. Random cross sections based on covariance of Figure 4.

campaign, for the PETALE analysis this perturbation isotope list might be enhanced together with the number of perturbations. Note that according to [9] and assuming a normal distribution, the confidence interval of a standard deviation is given by equation (1). Then using 32 random samples, the confidence interval is equal to 13% meaning that, for a propagated uncertainty of 10%, the 1σ confidence interval is between 8.7 to 11.3%, providing a good order of magnitude for a nuisance parameter.

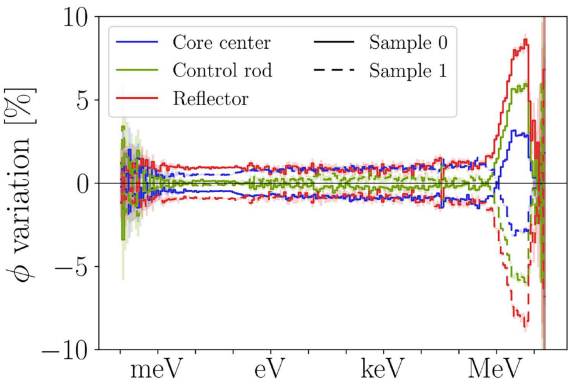

Fig. 6. Neutron spectrum variation (2 samples) in the different core regions using ENDF/B-VII.1.

$$\mathrm{std}^2_{\min} = \frac{(n-1)\mathrm{std}^2}{\chi^2_{1-(\alpha/2)}}, \quad \mathrm{std}^2_{\max} = \frac{(n-1)\mathrm{std}^2}{\chi^2_{(\alpha/2)}}. \quad (1)$$

For illustrative purposes, the spectrum variations of the first two samples are presented in Figure 6. We can see two kinds of results. The variation of the spectrum is changing according to energy: in order to represent this variation according to the 32 samples Figure 7 contains the relative standard deviation (rsd) using different nuclear databases. The second element is the direction of the variation between the samples (plain line or dashed line): in the fast range, all the regions (core center, control rod and reflector) are moving accordingly. The reflector (blue curve) is moving in the opposite direction compared to the other regions in the thermal and epithermal ranges. This information is contained in the covariance matrix presented in Figure 8 for the 32 samples. The variation of the flux in each region being related to the others, the covariance matrix is not limited to each region separately but all together.

When using the ENDF/B-VII.1 database (Fig. 7 top) in the high energy range, the uncertainty is of around 2.5% in the core center (blue curve) and larger than 6% in the reflector. The light red, blue and green lines are the relative standard deviation component due to the statistical uncertainty. This statistical component needs to be small enough (*i.e.* calculation long enough) to be negligible compared to the nuclear data uncertainty component. In the epithermal range, the relative standard deviation is lower than at high energy with ENDF/B-VII.1, and increases again in the thermal energy range. Comparing the tested nuclear databases ENDF/B-VII.1, ENDF/B-VIII.0 and JEFF-3.3, we can see that the relative standard deviation is changing a lot, especially in the high energy range (above 1 MeV) and also in the thermal range with a reduction in the uncertainty.

Thanks to these calculations, the uncertainty is propagated on the neutron spectrum. This uncertainty propagation loses the information on 'what is the origin of a specific effect, such as the larger uncertainty with ENDF/B-VII.1 at high energy compared to the other

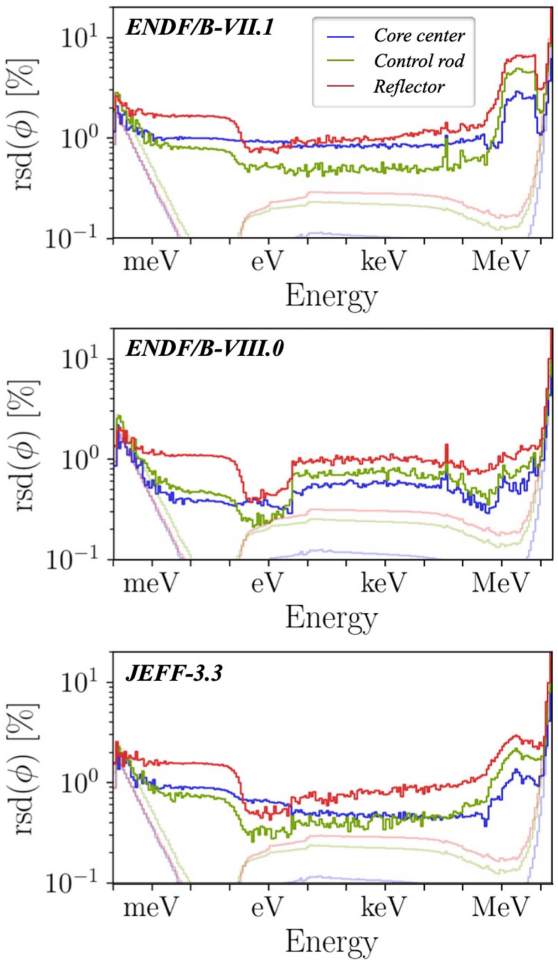

Fig. 7. Neutron flux relative standard deviation (32 samples) due to nuclear data uncertainty in the experimental positions, the shadow curves correspond to the pure statistical noise of the transport Monte Carlo calculations.

databases. However to estimate a nuisance parameter or to perform a Bayesian Monte Carlo assimilation, this information is not required.

Associated to this standard deviation, the correlation matrix (Fig. 8) provides the influence of a perturbation of a specific energy bin on the other bins. The correlation matrix is a 3×3 block matrix, each diagonal matrice corresponds to a single spectrum location correlation, and the other matrices correspond to the influence of a perturbation in a specific position (*e.g.* the core center) on the other positions (*e.g.* the reflector). We can see here for example that, for all the nuclear databases, an increase in the thermal flux component in the core center implies a decrease (negative correlation) in the neutron flux in the reflector.

3.1.3 Uncertainty propagation on the dosimeters

A classic Monte Carlo uncertainty propagation on the dosimeters would consist in estimating the reaction rate for these random ACE files for each irradiation configura-

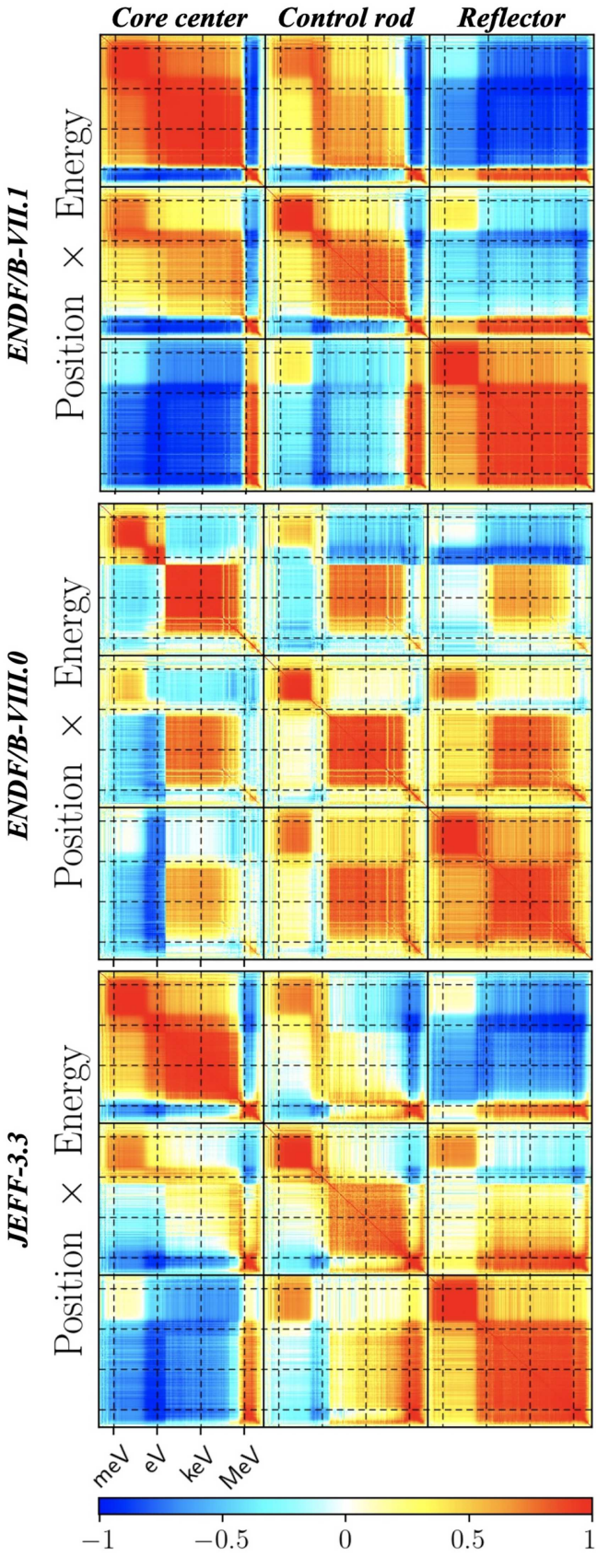

Fig. 8. Correlation matrices corresponding to the relative standard deviation of Figure 7.

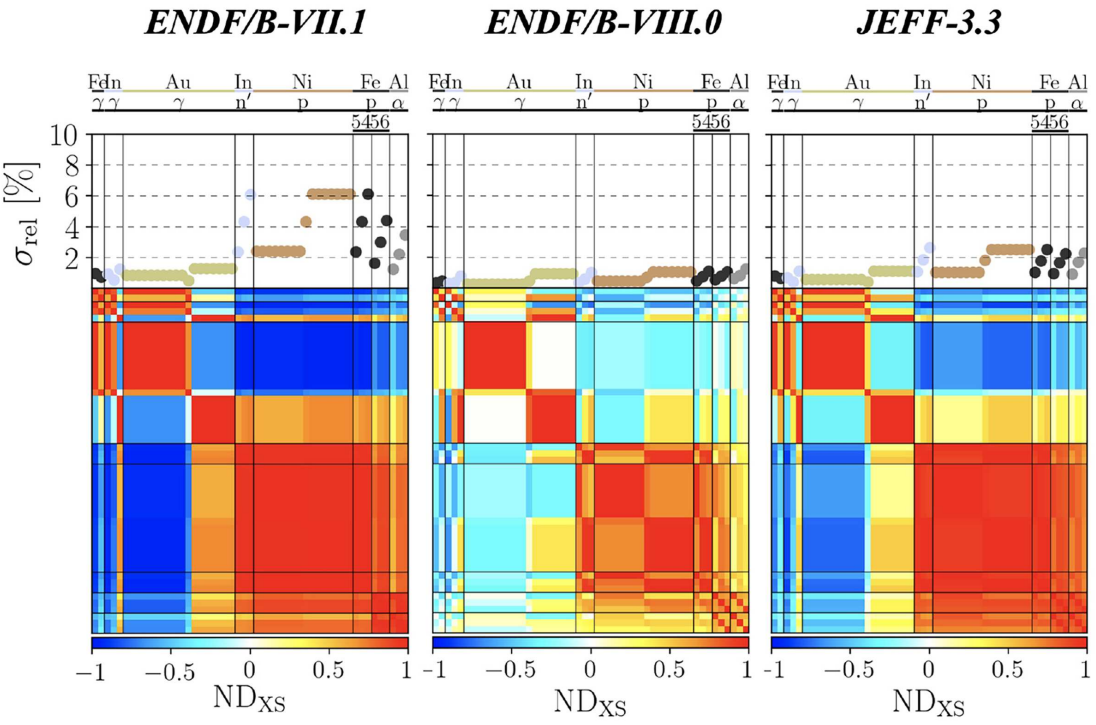

Fig. 9. Propagated nuclear data uncertainty on the dosimeter reaction rate using ENDF/B-VII.1 (left), ENDF/B-VIII.0 (middle) and JEFF-3.3 (right). The top plots are the standard deviation (1σ) for the different dosimeters and reactions on the x-axis. The bottom matrices are the correlation matrices associated with the standard deviation.

tion. However, this would require many different calculations if the number of irradiations is large and the effect of the nuclear data uncertainty is very similar in all the calculations, except if a strong self-shielding in the dosimeter interferes with the nuclear data uncertainty propagation. The approach used is based on the obtained relative standard deviation and correlation matrix (Figs. 7 and 8) associated with the sandwich rule formula on the reaction rate in the dosimeters. In this way, we can estimate the propagated uncertainty in a similar way as for the dosimetry IRDFF cross-section covariance matrices are detailed in [3].

Finally, we obtain a standard deviation for each dosimeter, plus a corresponding covariance matrix shown in Figure 9. All the measured dosimeters are settled here on the same x-axis, allowing a global overview of the propagated uncertainty. The first line is the relative standard deviation, each color corresponds to a type of dosimeter for a better understanding. For a given dosimeter, for example, the nickel in orange, three different values are visible with ENDF/B-VII.1: the first (∼2%) corresponds to the core center, the second (∼4%) to the control rod location and the third (∼6%) to the reflector position. Gold and nickel dosimeters take a larger part of the axis due to the axial measurement all along the plastic bars and then a larger number of measurements.

Depending on the nuclear database, the propagated uncertainty can be very different. In this study we obtain a much smaller uncertainty with ENDF/B-VIII.0 rather than with ENDF/B-VII.1, and an intermediate value with JEFF-3.3.

3.2 Efficiency ratio

During this measurement campaign, the neutron flux is lower at high energy in the reflector region compared to the core center as shown in Figure 3. However, the neutron flux is not that low since the dosimeters are settled close to the core. In the PETALE experimental program, some dosimeters are measured in the reflector region with 16 cm of metal reflector between the dosimeters and the core. For this reason, the reaction rate in these dosimeters is very low, and precise measurements are required.

For a given HPGe crystal with given timing constraints, the count rate can be improved using three different ways: a higher neutron flux (reactor power), a larger dosimeter size, or a smaller dosimeter to crystal distance. In CROCUS the maximal power is limited to 100 W and a large dosimeter size impacts the neutron flux and thus the measurement quality. The last aspect concerns the crystal-to-dosimeter distance and is illustrated in Figure 10. A large distance is characterized by a longer counting duration but it allows a precise calibration thanks to the very low probability of cascade effect (time-correlated emission of two γ-rays in the same decay chain). A short distance allows a faster measurement but is sensitive to the cascade effect that changes the apparent efficiency; this effect can be modeled for a well-known crystal even if this is adding external uncertainties. Note that the count rate (and coincidence) remains very low even for close measurements due to the low dosimeter activity.

For this reason, a methodology adapted to the PETALE measurement configuration has been developed,

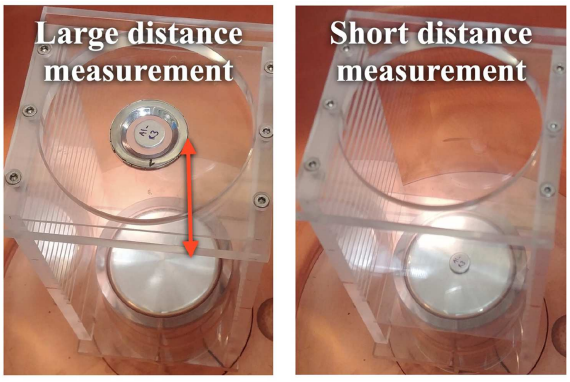

Fig. 10. Dosimeter positioning system far (left) and close (right) to the HPGe.

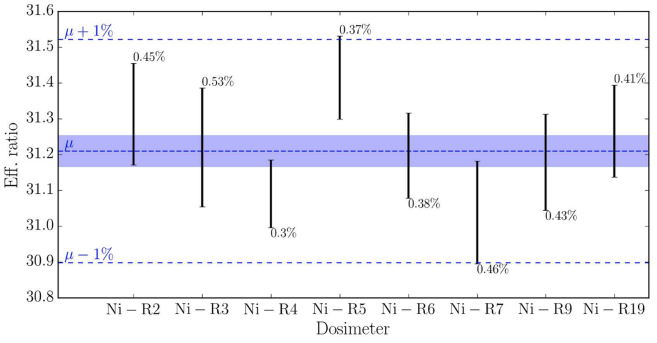

Fig. 11. Independent efficiency ratio measurements for nickel dosimeters.

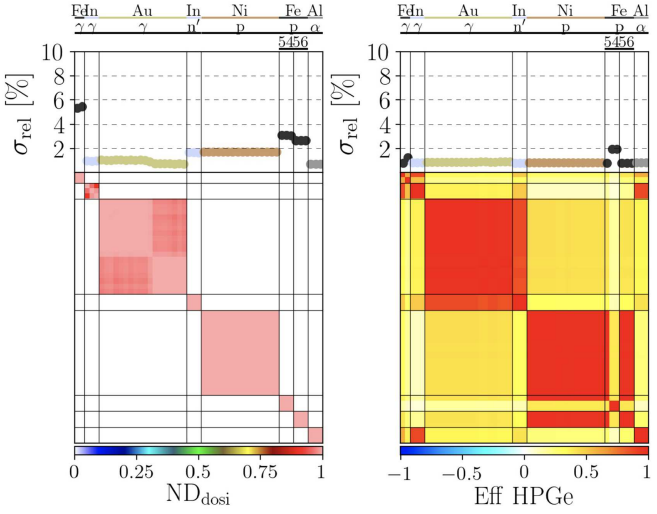

Fig. 12. Uncertainty component due to dosimetry reaction nuclear data uncertainties (left) and HPGE efficiency calibration including efficiency ratio when applied (right).

combining the advantages of both distances. For a given distance to the crystal, the cascade effect is not changing with the dosimeter activity, it only depends on the dosimeter geometry, material, and γ-ray energy emission. Then for a given set of dosimeters with a low expected count rate in the experimental setup, an identical dosimeter is settled in the core center and measured at both distances in the HPGe: the measurement ratio corresponds to the efficiency ratio taking into account the cascade effect. Thanks to this, the low-activity dosimeter only needs to be measured at a low distance (high efficiency) from the HPGe, the measured efficiency ratio converts the measurement to the large distance (low efficiency) where the calibration sources provide a precise efficiency calibration.

In order to validate this methodology, a series of independent irradiated dosimeters have been measured at the two distances from the HPGe and the efficiency ratios have been compared. The results obtained for the series of nickel dosimeters are presented in Figure 11. We can see that all the independent measurements are compatible with the combined value. Thanks to this technique, the efficiency ratio and the measurement time are improved by a factor of 31 for nickel dosimeters.

4 Calculation-experiment comparison

In order to compare the calculated and experimental values, two additional uncertainty components detailed in [3] are the nuclear data uncertainty due to the dosimetry cross section and the HPGe efficiency calibration. The corresponding standard deviation and correlation matrices for the experiment detailed in this paper are displayed in Figure 12.

Note that the efficiency ratio technique has been tested in the frame of this campaign using nickel dosimeters, but also used for the presented results for the ^{54}Fe and ^{58}Fe (n,p) reactions since the reaction rates in the control rod and reflector position are very low. The efficiency ratio measurements are based on the iron dosimeter irradiation at the core center to limit the statistical uncertainty. We can see that the standard deviation on the HPGe efficiency is larger for the corresponding control rod and reflector positions (back points below the Fe in the right matrix with a rsd from 1 to 2% in Fig. 12).

Finally, Figure 13 presents the "calculation/experiment" in percents for the different tested nuclear databases. We can see a good global agreement for the dosimeter sensitive to the thermal range on the left and an underestimation of the reaction rate for the high energy sensitive dosimeters on the right.

For the ENDF/B-VII.1 nuclear data library, the average value is better and, thanks to the nuclear data uncertainties, the results are compatible with a C/E = 1. However for JEFF-3.3 and ENDF/B-VIII.0 libraries, the average results are reduced and the strong reduction in the nuclear data uncertainties makes the C/E incompatible with 1. A remaining uncertainty component to add to the analysis is the fission neutron emission spectrum which is not sampled yet and might explain a part of the discrepancies at high energy.

Even for the dosimeters with a bias of around 5% such as nickel, we can see that this is a systematic bias on the absolute value (*i.e.* the agreement between two

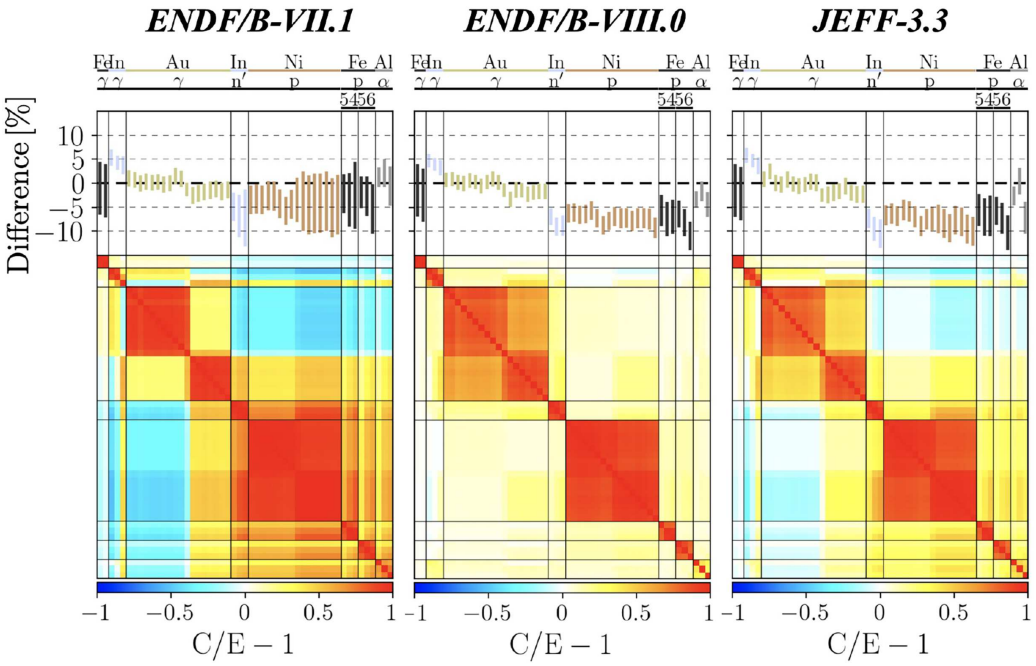

Fig. 13. Calculation-experiment comparison using ENDF/B-VII.1 (left), ENDF/B-VIII.0 (middle) and JEFF-3.3 (right). The top plots are the reaction rate difference between the calculations and the measurements on the x-axis, the thickness is the combined uncertainty (1σ) for the different dosimeters and reactions. The bottom matrices are the correlation matrices associated with the standard deviation.

dosimeters is very good). This is an expected element highlighting that transmission experiment through metal plates in PETALE with a strong correlation allows reducing the global uncertainty by internal comparison in between the dosimeters.

5 Conclusions and perspectives

The measurements presented succeed to characterize the local neutron flux in the CROCUS reactor and to test the analysis procedure for the incoming PETALE experimental program. Two analysis procedures have been settled and tested: the efficiency ratio and the nuclear data uncertainty propagation up to the dosimeter reaction rates.

The efficiency ratio technique presented here allows to significatively reduce the HPGe measurement time for dosimeters irradiated in low neutron flux region. This technique can be applied if an equivalent (shape and reaction) dosimeter is irradiated in a high flux region. It can be applied to the PETALE program: the efficiency ratio being is measured with a dosimeter settled in the core center, and then applied for dosimeters in the metal reflector.

The nuclear data uncertainty propagation based on a Monte Carlo sampling of the cross-section ACE files is an applicable solution for dosimetry applications. It consists in generating the cross-section covariances using NJOY, sampling multiple ACE files, using these cross-sections in different neutron transport calculations to obtain different flux spectra and then the spectrum covariance, and propagating this covariance on the dosimeter reaction rates. For the PETALE program, the approach can be applied between the metal plates to estimate the uncertainty on the neutron spectrum at the different positions in the reflector including the correlation in-between the dosimeter positions. The number of perturbed isotopes in the core can also be increased together with the reactions in order to include all the contributions to the experimental uncertainty.

Conflict of interests

The authors declare that they have no competing interests to report.

Funding

This research did not receive any specific funding.

Data availability statement

This article has no associated data generated and/or analyzed/Data associated with this article cannot be disclosed due to legal/ethical/other reason.

Author contribution statement

Axel Laureau carried out the model development and numerical implementation, with the help of Vincent Lamirand for the experimental aspects related to CROCUS and the project management on EPFL side, Adrien Gruel for the project management on the CEA side, Alix Sardet for experimental aspects related to dosimetry and Thomas Ligonnet for the improvement of

the estimation of the measurement precision. Andreas Pautz supervises the EPFL laboratory. All authors discussed the results and contributed to the final manuscript.

References

1. V. Lamirand, G. Perret, S. Radman, D. Siefman, P. Frajtag, M. Hursin, A. Gruel, P. Leconte, P. Blaise, A. Pautz, Design of separated element reflector experiments in crocus: Petale, in *Reactor Dosimetry: 16th International Symposium* (ASTM International, 2018)
2. V. Lamirand, A. Laureau, D. Rochman, G. Perret, A. Gruel, P. Leconte, P. Blaise, A. Pautz, An experimental programme optimized with uncertainty propagation: Petale in the crocus reactor, EPJ Web Conf. **211**, 03003 (2019)
3. A. Laureau, V. Lamirand, A. Gruel, P. Frajtag, A. Pautz, Dosimetry modeling and experimental validation for the petale program in the crocus reactor, EPJ Web Conf. **247**, 08015 (2021)
4. J. Leppänen, M. Pusa, T. Viitanen, V. Valtavirta, T. Kaltiaisenaho, The Serpent Monte Carlo code: Status, development and applications in 2013, Ann. Nucl. Energy **82**, 142–150 (2015)
5. A. Laureau, V. Lamirand, D. Rochman, A. Pautz, Total monte carlo acceleration for the petale experimental programme in the crocus reactor, EPJ Web Conf. **211**, 03002 (2019)
6. E. M. Zsolnay, N. Capote, H. J. Nolthenius, A. Trkov, et al., Summary description of the new international reactor dosimetry and fusion file (irdff release 1.0), Tech. rep., International Atomic Energy Agency (2012).
7. A. Laureau, V. Lamirand, D. Rochman, A. Pautz, Bayesian monte carlo assimilation for the petale experimental programme using inter-dosimeter correlation, in *The International Conference on Nuclear Data for Science and Technology, ND2019*, China (2019)
8. R. Macfarlane, D. W. Muir, R. Boicourt, A. C. Kahler III, J. L. Conlin, The njoy nuclear data processing system, version 2016, Tech. rep., Los Alamos National Lab.(LANL), Los Alamos, NM (United States) (2017)
9. D. J. Sheskin, *Handbook of Parametric and Nonparametric Statistical Procedures* (Chapman and Hall/CRC, 2003).

Cite this article as: Axel Laureau, Adrien Gruel, Vincent Lamirand, Thomas Ligonnet, Alix Sardet, and Andreas Pautz. Analysis of the preliminary campaign for the PETALE program, EPJ Nuclear Sci. Technol. **9**, 25 (2023)